



# Bright Band Simulations using WRF Model with New Melting Microphysics

T. Iguchi<sup>1,2</sup>, T. Matsui<sup>1,2</sup>, W.-K. Tao<sup>1</sup>, A. P. Khain<sup>3</sup>, V. T. J. Phillips<sup>4</sup>, C. Kidd<sup>1,2</sup>,

T. L'Ecuyer<sup>5</sup>, S. A. Braun<sup>1</sup>, and A. Y. Hou<sup>1</sup>



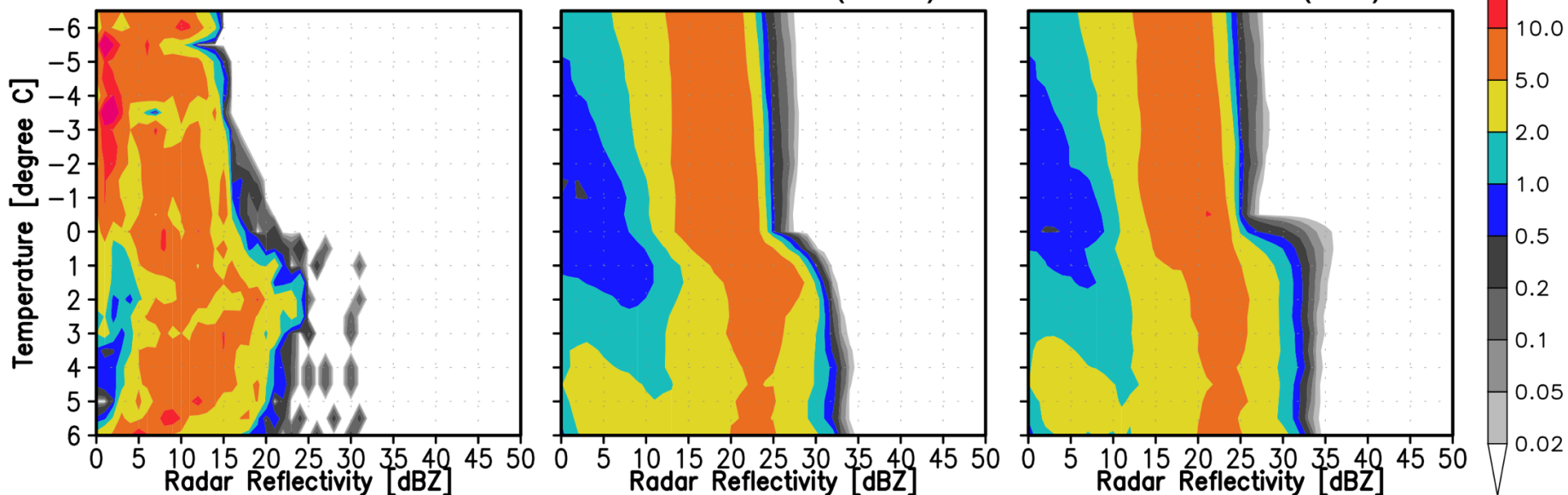
<sup>1</sup>Code 612 NASA/GSFC, <sup>2</sup>ESSIC UMD, <sup>3</sup>Hebrew University, <sup>4</sup>Lund University, and <sup>5</sup>University of Wisconsin

## K-band dBZ CFTDs (%) on Oct 20, 2010

Observation

WRF-SBM (new)

WRF-SBM (old)



Normalized contoured frequency by temperature diagrams (**CFTDs**) highlight peak radar reflectivity in **bright bands** in a temperature range of 0 – 3 °C. The Weather Research and Forecasting model coupled with spectral bin cloud microphysics (**WRF-SBM**) simulated a mixed-phase precipitation event using two types of ice melting model: a **new gradual ice-melting model** and an old instantaneous melting model. The new model improved simulation of peak reflectivity profiles in a bright band.



Name: Takamichi Iguchi, NASA/GSFC, Code 612 / ESSIC, University of Maryland  
E-mail: Takamichi.Iguchi@nasa.gov  
Phone: 301-614-6225



## References:

T. Iguchi, T. Matsui, W.-K. Tao, A. P. Khain, V. T. J. Phillips, C. Kidd, T. L'Ecuyer, S. A. Braun, and A. Hou, 2014: WRF-SBM Simulations of Melting-Layer Structure in Mixed-Phase Precipitation Events Observed during LPVEx. *Journal of Applied Meteorology and Climatology*, **53**, 2710–2731.  
doi: <http://dx.doi.org/10.1175/JAMC-D-13-0334.1>

**Data Sources:** The Weather Research and Forecasting model coupled with spectral bin cloud microphysics (WRF-SBM) simulations were driven by an interim global atmosphere reanalysis produced by the European Centre for Medium-Range Weather Forecasts (ERA-interim). Vertically pointing Micro Rain Radar (MRR) data was collected during the Light Precipitation Validation Experiment (LPVEx) campaign. Sounding data at the Jokioinen site was provided by the Department of Atmospheric Science of the College of Engineering at the University of Wyoming.

## Technical Description of Figures:

**Bright bands in CFTD:** “Bright band” is a phenomenon recognized as a layer with relatively high radar reflectivity below the 0 °C temperature level in a radar echo profile. The high reflectivity is caused by several factors related to melting of falling ice particles in the layer. Normalized contoured frequency by temperature diagrams (CFTDs) of K-band radar reflectivity factors show vertical structure of cloud and precipitation in a form more highlighting ice-melting layers. Observation CFTDs were calculated from vertical radar reflectivity profiles obtained by a MRR deployed at the Jarvenpaa site and sounding temperature data at the Jokioinen site. Simulation CFTDs were calculated from temperature and radar reflectivity distribution in WRF-SBM simulations; the radar reflectivity is simulated through the Goddard Satellite Simulator Unit (G-SDSU). Two types of WRF-SBM simulation were conducted for the same precipitation events: One used a new ice-melting cloud microphysics scheme, in which cloud ice particles gradually melted as prognostic melting volume fractions change. Another used an old ice-melting scheme, in which ice particles instantaneously melted when entering layers warmer than 0 °C temperature. A common relatively high reflectivity part in a temperature range of 0 – 3 °C can be found in the CFTDs of both observation and simulation only with the new scheme. In contrast, no corresponding high reflectivity part appears in the simulation plots with the old scheme. These results show a good demonstration of the state-of-the-art modeling of ice melting process for simulation of bright band structure in atmospheric models.

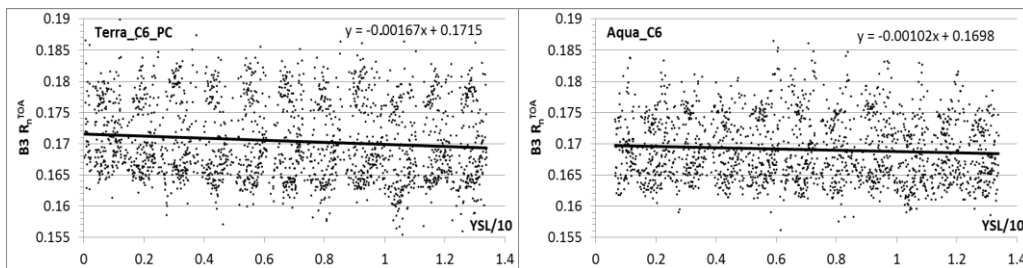
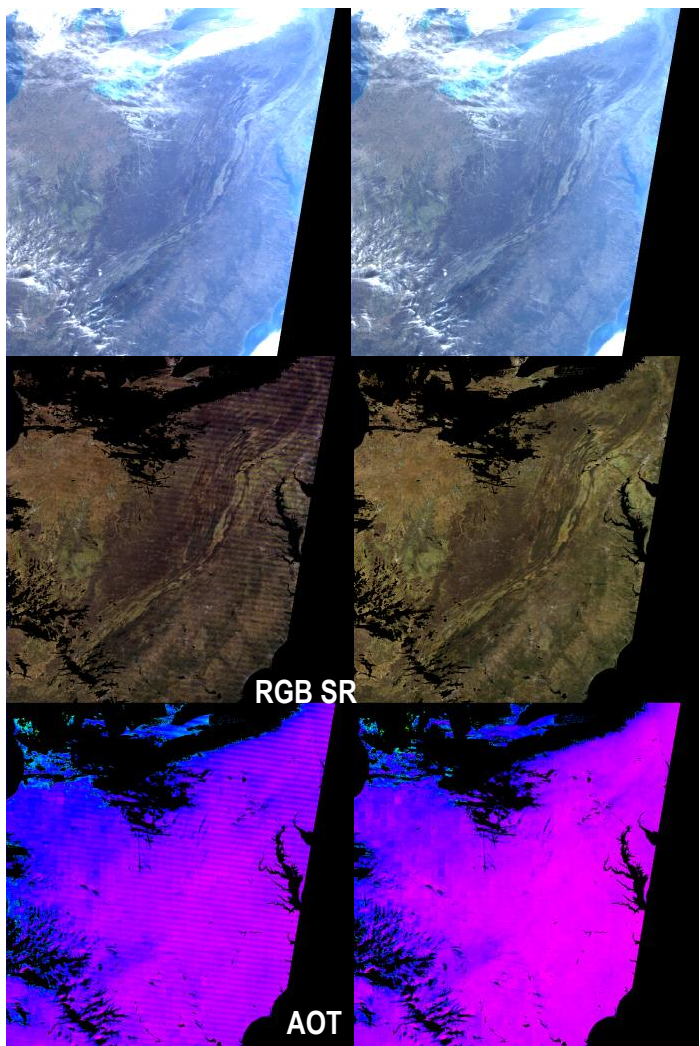
**Scientific significance, societal relevance, and relationships to future missions:** Better understanding of bright bands is a key to reducing errors in an estimate of rainfall rates from satellite measurements such as the Tropical Rainfall Measuring Mission (TRMM) and the Global Precipitation Measurement (GPM); a high backscattering signal in bright bands may be mistakenly interpreted as the existence of a high rainfall rate. Exact representation of bright bands is a significant challenge in high-resolution atmospheric simulation with detailed cloud microphysics model. It supports comprehensive investigation of their formation mechanisms related to a gradual change of the melting volume fractions of falling ice particles and their complicated scattering properties at a radar beam wavelength. In addition, model simulation data can be utilized to construct full three-dimensional depictions of precipitation scenes that cannot be obtained from a single in-situ or remotely sensed measurement. The WRF-SBM model has been integrated into a synthetic simulator for GPM ground validation programs. The simulation results can be used to provide testbed databases supporting the development of various rainfall retrieval algorithms. WRF-SBM simulation data for these precipitation scenes in LPVEx will be available to the research community through the Cloud Library data portal.



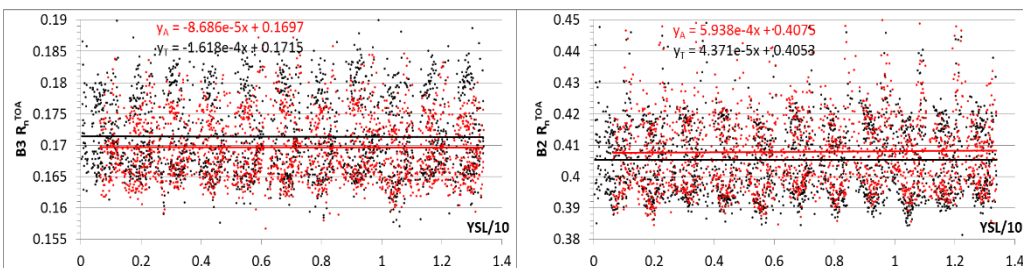
# MODIS Terra-Aqua C6+ Cross-Calibration Improvements

Lyapustin<sup>1</sup>, X. Xiong<sup>2</sup>, Y. Wang<sup>3</sup>, G. Meister<sup>4</sup>, S. Platnick<sup>5</sup>, R. Levy<sup>1</sup>, B. Franz<sup>4</sup>, A. Wu<sup>6</sup>, A. Angal<sup>6</sup>

<sup>1</sup>Code 613; <sup>2</sup>Code 618; <sup>4</sup>Code 616; <sup>5</sup>Code 610 NASA GSFC; <sup>3</sup>UMBC; <sup>6</sup>SSAI



a) Trends in MODIS C6 blue channel (B3, 0.47  $\mu\text{m}$ ) from MODIS on Terra and Aqua observed over Libya4 site over time (in Years Since Launch)



b) De-trended data in the Blue (B3) and near-IR (B2, 0.87  $\mu\text{m}$ ) show a clear gain offset between MODIS Terra (black) and Aqua (red)

*GSFC-led work further improves calibration of MODIS Collection 6 record. The C6+ adds correction of changing polarization sensitivity of MODIS Terra, removal of residual trends, and cross-calibration gain adjustment between Terra and Aqua. The cross-calibration of sensors on different orbits is achieved via a novel way using geometric (BRDF) normalization.*

Polarization correction (right) removes artifacts in C6 MODIS Terra Surface Reflectance and AOT



Name: Alexei Lyapustin, NASA/GSFC Code 613  
E-mail: Alexei.I.Lyapustin@nasa.gov  
Phone: 301-614-5998

### References:

Lyapustin, A., Y. Wang, X. Xiong, G. Meister, S. Platnick, R. Levy, B. Franz, S. Korokin, T. Hilker, J. Tucker, F. Hall, P. Sellers, A. Wu, A. Angal (2014), Science Impact of MODIS C5 Calibration Degradation and C6+ Improvements, *Atmos. Meas. Tech.*, 7, 4353-4365.

Kwiatkowska, E.J., B.A. Franz, G. Meister, C.R. McClain, and X. Xiong (2008). Cross calibration of ocean-color bands from Moderate Resolution Imaging Spectroradiometer on Terra platform, *Appl. Opt.*, 47(36), 6796-6810.

Lyapustin, A., Y. Wang, I. Laszlo, T. Hilker, F. Hall, P. Sellers, J. Tucker, S. Korokin, 2012: Multi-Angle Implementation of Atmospheric Correction for MODIS (MAIAC). 3: Atmospheric Correction. *Rem. Sens. Environ.*, <http://dx.doi.org/10.1016/j.rse.2012.09.002>.

Sun, J., X. Xiong, A. Angal, H. Chen, A. Wu, and X. Geng: Time-Dependent Response Versus Scan Angle for MODIS Reflective Solar Bands, *IEEE Trans. Geosci. Remote Sensing*, 52(6), 3159-3174, 2014.

**Data Sources:** MODIS Terra and Aqua Level 1B data.

### Technical Description of Figures:

**Image:** Improvements from polarization correction (PC) of MODIS Terra C6 L1B data (right) compared to uncorrected data (left) for day 349, 2012. PC removes 10km striping in MAIAC AOT (bottom) and spectral distortions in RGB surface reflectance (middle). The measured top-of-atmosphere reflectance is shown on top.

**Graph a):** Clear-sky daily top-of-atmosphere reflectance over Libya4 site as a function of Years Since Launch (YSL)/10. is computed for the fixed geometry of nadir view and 45° solar zenith angle based on MAIAC products (cloud mask, column water vapor, aerosol optical thickness, spectral surface BRDF).

**Graph b):** Daily MODIS Terra (black) and Aqua (red) reflectance over Libya4 site after de-trending.

**Scientific significance, societal relevance, and relationships to future missions:** The latest assessment of the calibration-related artifacts in MODIS Terra C5 products reveal global decreasing decadal trends of ~27% aerosol optical thickness, ~17% cloud optical thickness, and ~0.01 normalized difference vegetation index (NDVI) over land (Lyapustin et al., 2014). The C6 calibration (Sun et al., 2014) removed major calibration trends. In this work we further improved C6 calibration by adding: a) polarization correction of MODIS Terra based on polarization sensitivity coefficients provided by the GSFC Ocean Biology Processing Group (Kwiatkowska et al., 2008); and v) de-trending of both Terra and Aqua and their cross-calibration (graphs a-b) based on analysis of MAIAC (Lyapustin et al., 2012) processing over stable desert “calibration” sites. MAIAC science analysis over the southern USA showed that the enhanced C6+ calibration improved agreement between Terra and Aqua decadal NDVI change by a factor of 3 (Lyapustin et al., 2014). Currently, C6+ calibration is being used in the MODIS Land discipline C6 re-processing, while the atmospheric (aerosol) global analysis is underway. This work is directly related to major NASA missions by improving sensor calibration and long-term stability, providing climate-quality data record for the Earth Sciences and applications.

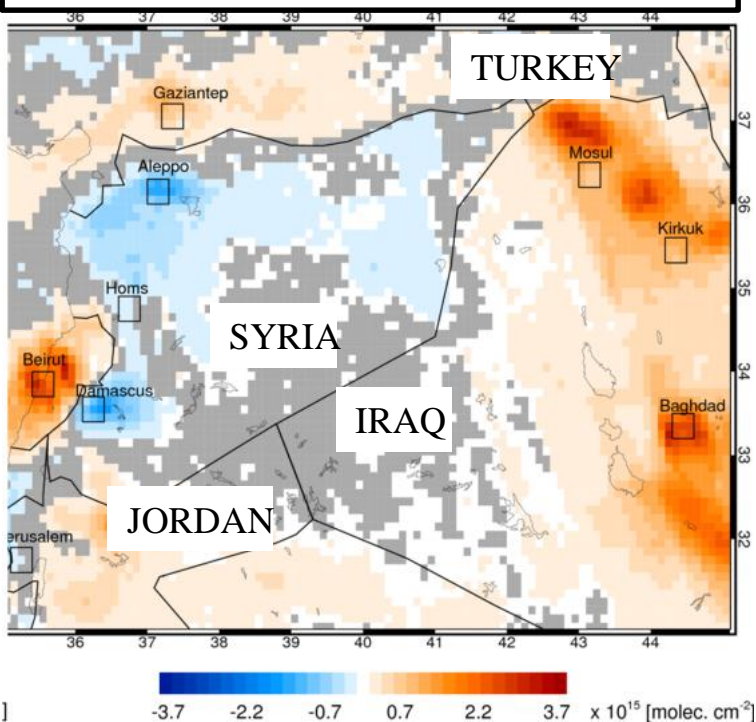


# Aura OMI NO<sub>2</sub> data: Regional changes in air pollution

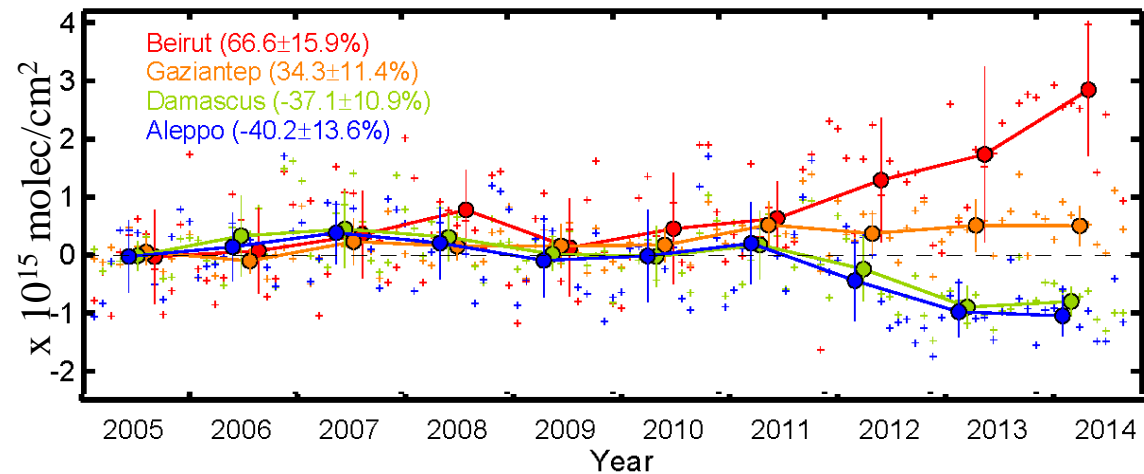


Bryan Duncan, Lok Lamsal, Anne Thompson, Yasuko Yoshida, Maggie Hurwitz, Ken Pickering (614)

NO<sub>2</sub> Changes (molec/cm<sup>2</sup>): 2005-2014



Deseasonalized NO<sub>2</sub> Changes (molec/cm<sup>2</sup>): 2005-2014



Economic changes and migration within the Middle East has led to major changes in the distribution of air pollution as shown by Aura OMI NO<sub>2</sub> data.



Name: Bryan Duncan, NASA/GSFC, Code 614  
E-mail: Bryan.N.Duncan@nasa.gov  
Phone: 301-614-5994



**Reference:** Duncan, B.N., L.N. Lamsal, A.M. Thompson, Y. Yoshida, Z. Lu, D.G. Streets, M.M. Hurwitz, and K.E. Pickering, *A space-based, high-resolution view of notable changes in urban NO<sub>x</sub> pollution around the world (2005-2014)*, under review, *J. Geophysical Research*, 2015

**Data Sources:** Aura Ozone Monitoring Instrument (OMI) data of Nitrogen Dioxide (NO<sub>2</sub>).

### Technical Description of Figures:

**Map (a):** Absolute difference of annual average OMI NO<sub>2</sub> data ( $\times 10^{15}$  molecules/cm<sup>2</sup>; 0.1° latitude  $\times$  0.1° longitude) between 2005 and 2014. Warmer colors indicate increases and cooler colors represent decreases. Gray areas represent where there are no statistically significant changes.

**Map (b):** De-seasonalized OMI NO<sub>2</sub> data ( $\times 10^{15}$  molecules/cm<sup>2</sup>) for several Middle Eastern cities. Monthly and annual average values are shown as pluses (+) and circles, respectively. Vertical bars on the annual average values represent the standard deviation for a given year.

**Scientific significance, societal relevance, and relationships to future missions:** There were major changes in air pollution around the world as discussed in Duncan et al. [2015]. We use high-resolution nitrogen dioxide (NO<sub>2</sub>) data from the OMI to analyze changes in urban NO<sub>2</sub> levels around the world from 2005 to 2014, finding complex heterogeneity in the changes. We show the potential of high-resolution data for quantifying NO<sub>x</sub> emissions in regions with a complex mix of sources. NO<sub>2</sub> is produced during combustion processes and, thus, may serve as a proxy for changes in fossil fuel-based energy usage and co-emitted greenhouse gases, such as CO<sub>2</sub>, and other pollutants.

We found that NO<sub>x</sub> changes were determined by several factors: First, environmental regulations resulted in large decreases. The only large increases in the United States occurred over three areas of intensive energy activity. Second, rapid economic growth elevated NO<sub>2</sub> levels over many Asian, tropical and subtropical cities. Two of the largest increases occurred over recently expanded petrochemical complexes in Jamnagar (India) and Daesan (Korea). Third, pollution transport from China influenced the Republic of Korea and Japan, diminishing their local emission controls. However, in China, there were large decreases over Beijing, Shanghai, and the Pearl River Delta, associated with local emission control efforts. Fourth, civil unrest and its effect on energy usage resulted in lower NO<sub>2</sub> levels in some countries. Fifth, spatial heterogeneity within several megacities reflects mixed efforts to cope with air quality degradation.

Intensive monitoring of the world's tropical/subtropical megacities will remain a priority as their populations and emissions of pollutants and greenhouse gases are expected to increase significantly (>2 billion by 2050).